Journal of Cluster Science (2019) 30:937–946
https://doi.org/10.1007/s10876-019-01551-6

ORIGINAL PAPER

Biofabrication of Zinc Oxide Nanoparticles from *Aspergillus niger*, Their Antioxidant, Antimicrobial and Anticancer Activity

Yu Gao[1] · Mariadoss Arokia Vijaya Anand[2] · Vinayagam Ramachandran[2] · Venkatachalam Karthikkumar[3] · Vijayakumar Shalini[2] · Sankaran Vijayalakshmi[2] · David Ernest[2]

Received: 7 March 2019 / Published online: 12 April 2019

Abstract

The present study was aimed to green synthesis and characterization of zinc oxide nanoparticles (ZnONPs) from *Aspergillus niger,* which was evaluated for their antioxidant, antimicrobial and anticancer activity. The synthesised NPs were characterized by various analytical techniques such as UV–VIS Spectroscopy, FT-IR, XRD, DLS, SEM, and TEM. It was confirmed through the UV–Vis spectrophotometer; corresponding peaks were identified at 390 nm. The green synthesised ZnONPs were characterized by FT-IR studies to reveal the functional group attributed to the formation of ZnONPs. Morphological size of ZnONPs was 80–130 nm found through characterization by DLS, SEM, and TEM. Furthermore, the green synthesised ZnONPs showed potent antioxidant (ABTS and DPPH assay) antimicrobial activity against human pathogenic bacterial strains such as *Klebsiella pneumoniae, Escherichia coli, Pseudomonas aeruginosa,* and *Enterobacter aerogenes*. In addition, the green synthesised ZnONPs showed the dose-dependent cytotoxicity and apoptotic features in human hepatocellular carcinoma cells (HepG2). The overall findings of the study suggested that *A. niger* had a potential for the biosynthesis of ZnONPs as an alternative biomaterial for future therapeutic application as an antioxidant, antimicrobial and anticancer compound.

Keywords *Aspergillus niger* · Zinc oxide nanoparticles · HepG2 cell lines · Antioxidant · Antimicrobial · Anticancer

Introduction

Nanoparticles (NPs) are widely applied in medicine, cosmetics, and industries. NPs wide dimension between 1 and 1000 nm in size, they consist of macromolecular materials in which the active ingredient (drug or biologically active material) is dissolved, entrapped, or encapsulated or adsorbed [1]. Metal NPs have been intensively studied in the past decade. Biological systems have well organized and controlled physiological processes and thus, their use in the NPs synthesis is rapidly gaining importance. The concern is still expressed about potential hazardous effects of metal NPs, especially in the case of silver nanoparticles which seem to be the most toxic ones among other metals [2].

Zinc oxide nanoparticle (ZnONPs) has received considerable attention due to their unique antibacterial, antifungal, and anticancer activities. ZnONPs are also been excellent used for drug carrier systems. ZnONPs larger than 100 nm is considered to be relatively biocompatible, which supports their use for drug delivery and useful physical properties such as conductive coating efficacy [3]. ZnONPs contain an essential trace metal and have several advantages such as clinical applicability, consistent, wide band gap, photoluminescence, and predictable antioxidant properties which is very helpful in the preparation of ZnONPs. In addition, ZnO materials are low cost, low toxicity and biomedical applications such as targeted drug

✉ David Ernest
ernestdavid2009@gmail.com

[1] Department of General Surgery, Tianjin First Central Hospital, Tianjin 300204, China

[2] Department of Biotechnology, Thiruvalluvar University, Serkadu, Vellore, Tamil Nadu 632 115, India

[3] Department of Pharmacology and Therapeutics, College Of Medicine and Health Sciences, UAE University, Al Ain, United Arab Emirates

delivery [4]. Furthermore, ZnONPs has a highly promising potential in biological function such as the pharmaceutical sector, medical diagnostics, gene delivery, drug delivery, and nano-medicine along with anticancer, antibacterial and anti-diabetic activities [5].

The *Aspergillus* genus belongs to the fungi that are commonly found in various environments. However, only a few species of *Aspergillus* have a significant impact on human or animal health [6, 7]. *A. niger*, the most abundant mold found in the environment has also been the source of several bioactive compounds and industrial enzymes [8]. It is a haploid filamentous fungus which is used for waste management and biotransformation in addition to its industrial uses, such as the production of citric acid and extracellular enzymes [9]. Recent studies revealed that the antimicrobial activity of silver nanoparticles produced from *E. coli* is more pronounced than that of *A. niger* associated silver nanoparticles [10, 11]. Therefore, the present study was attempted for the synthesis and characterization of the ZnONPs by *A. niger* to be applied for cytotoxic and anticancer activities.

Materials and Method

Cells, Reagents, and Chemical

Zinc acetate, Minimum Essential Medium (MEM), Fetal bovine serum (FBS), Streptomycin, DCFH-DA, Acridine orange/Ethidium bromide, Ascorbic acids, 1,2-diphenyl-1-picrylhydrazyl and DAPI were purchased from Himedia, Mumbai. All other chemicals and solvents were obtained from S.D Fine Chemical, Mumbai and Fisher Inorganic and aromatic Limited, Chennai. Drug resistant-clinical strain of *Klebsiella pneumoniae, Escherichia coli, Pseudomonas aeruginosa,* and *Enterobacter aerogenes* were obtained from Sri Narayani Hospital & Research Centre, Vellore, Tamil Nadu, India. Hamster kidney fibroblast cells (BHK-21), Human Liver carcinoma cell lines (HepG2) were purchased from National Centre for Cell Science (NCCS), Pune, India.

Collection of Sample

The marine fungus, *A. niger* was isolated from the marine sediments of Appa Island in the Gulf of Mannar, India (8°35′N–9″29′N lat and 78°8′E–79°30′E long). The fungal strains were identified on the basis of their morphological, biochemical and molecular examinations. The isolated fungal strain was grown and maintained on potato dextrose agar plates at 28 °C and preserved as agar slants at 4 °C.

Green Synthesis of ZnONPs Using *A. niger*

A. niger was grown in enrichment medium containing 7 g of potassium dihydrogen phosphate (KH_2PO_4) 2 g of dipotassium phosphate (K_2HPO_4), 0.1 g of magnesium sulfate heptahydrate [$MgSO_4.7H_2O$]; 1.0 g of [$(NH_4)_2SO_4$], 0.6 g of yeast extract; and 10 g of glucose. To the 250 mL of liquid media, a loop full of *A. niger* was taken from a mother culture and inoculated and incubated at 28 °C on a rotary shaker at 200 rpm for 96 h. After incubation, the biomass was filtered using Whatman No. 1. Approximately 20 g of biomass was taken in the flasks containing 100 mL of sterile Milli-Q deionized water. The flasks were incubated under the same conditions described above for 24 h. The biomass was then filtered and the cell-free filtrate was collected. For the synthesis of ZnONPs, 50 mL of 1 mM of Zinc acetate was prepared deionized water and then continuously stirred for 24 h. After the incubation time, creamy-white precipitates of ZnONPs were formed. Then the precipitate was collected and dried at 150 °C for 48 h. The mycosynthesised NPs were eventually collected and subjected to subsequent studies.

Characterization of ZnONPs

The spectral absorption of green synthesised ZnONPs was analyzed by UV–visible spectrophotometer (Elico SL 196, Hyderabad, India). Fourier transfer infrared (FTIR) spectra were obtained on a Bruker Tensor 37 (FTIR Perkin Elmer Paragon 500, USA) and the X-ray diffraction pattern (XRD) were recorded using an Ultima IV X-ray diffractometer (X'pert-pro MPD-PANalytical, Netherland) at the angle range of 2θ (10°–80°). The particle size and topological features of the nanoparticles were recorded by Dynamic Light Scattering (DLS) [Horiba-DLS-7100E, Japan], Scanning Electron Microscope (SEM) (JEOL, Tokyo, Japan) and Transmission Electron Microscope (JEOL-JSM 1200EX, Japan).

Antioxidant Activity by the Myco-Synthesised ZnONPs

2,2′-azino-bis(3-ethylbenzothiazoline-6-sulfonic acid (ABTS) radical scavenging activity of ZnONPs was assessed by $ABTS^{\bullet+}$ cation decolorization and the absorbance was spectrophotometrically at 734 nm [12] $DPPH^{\bullet}$ radical scavenging activity of ZnONPs was measured according to the method of Shimada et al. [13]. The unit of total antioxidant activity is defined as the concentration of ascorbic acid having equivalent antioxidant activity expressed as μmol/g ZnONPs [13]. The percentage of

antioxidant activity was calculated by the subsequent equation:

$$\text{Antioxidant activity}(\%) = (A_0 - A_1)/A_0 \times 100$$

where A_0 absorbance of blank, A_1 absorbance of ZnONPs/ascorbic acid.

Antimicrobial Activity of Myco-Synthesised ZnO Nanoparticles

Pathogenic gram-negative drug resistant bacterial strain was used to evaluate the antimicrobial activities. The well diffusion assay was executed to screen the antimicrobial activity of mycosynthesised ZnONPs [14]. Muller Hinton agar was prepared and 50 µL fresh bacterial cultures were spread on the agar plate. The well was made in 5 mm diameter of the plates using gel puncher then the wells were loaded with different concentration of ZnONPs (50–500 µg). Streptomycin (1 mg/mL) was used as a positive control. The plates were incubated at 37 °C for 24 h and the zone of inhibition was measured in terms of the millimeter.

Screening of Membrane Leakage of Proteins and Nucleic Acid

The bactericidal effect of ZnONPs on membrane damage of protein and nucleic acid released from the cytoplasm of the cells after treatment with ZnONPs was estimated by the colorimetric method. 100 mL LB broth containing bacterial culture (*E. coli, P. aeruginosa, K. pneumoniae, and E. aerogenes*) was treated with 500 µL ZnONPs and incubated at 37 °C in the orbital shaker at 125 rpm. After 24 h, the culture was centrifuged at 10,000×*g* for 30 min at 4 °C and the supernatant was frozen at − 20 °C until assay. This sample is used for the estimation of proteins and nucleic acid. The protein leakage assay was accomplished using the method proposed by Kim et al. [15] and the nucleic acid leakage study was executed by the method Alvarez-Ordonez et al. [16] with little modifications. These experiments were done in triplicate.

Cell Culture and Cytotoxicity Analysis

HepG2 cell lines (liver cancer cell line) and Human embryonic kidney cell line of HEK-293 (Non-cancerous) were procured from the National Center for Cell Sciences (NCCS), Pune, India. The cells were cultured in MEM medium supplemented with FCS and 2 mM L-glutamine and balanced salt solution (BSS). The growth medium was supplemented with 10% fetal bovine serum (FBS), penicillin and streptomycin (100 IU/100 µg). The cells were sustained at 37 °C in a 5% CO_2 humidified atmosphere. Cytotoxic potential of ZnONPs was estimated by 3-(4,5-dimethylthiazol-2-yl)-2,5-diphenyltetrazolium bromide (MTT) assay [17]. Briefly, HepG2 and HEK-293 cells (5000 cells/well) were seeded into 96-well plates and incubated for 24 h. The cells were washed with PBS then replaced with fresh medium. Then the cells were treated with different concentration (10, 20, 30, 40 and 50 µg/mL) of ZnONPs and incubated for 24, 48 and 72 h. The cell proliferation was then assessed by performing MTT assay as described by Hansen et al. [17]. The results were compared with a noncancerous cell line of HEK-293 and positive control of doxorubicin.

Morphological Detection of Apoptosis Using Dual Staining

Morphological examination of apoptotic features in ZnONPs treated HepG2 cell was done by AO/EtBr staining. Briefly, HepG2 cells (2×10^4) were cultured in 6 well plates treated with IC_{50} concentrations of ZnONPs for 24, 48 and 72 h, then washed with PBS. Then 10 µL of 1 mg/mL of AO/EtBr was added to each well. Doxorubicin-treated cells were used as positive control. The apoptotic changes were visualized and photographed by fluorescence microscope (Nikon Eclipse, Inc, Japan).

Analysis of Nuclear Damage Using DAPI Staining

HepG2 cells (1×10^6 cells/well) were grown on a tissue culture plate and treated with IC_{50} concentrations of ZnONPs for 24, 48, and 72 h. Doxorubicin-treated cells were used as a positive control after the incubation, the cells were harvested and washed with cold PBS. The cells were permeabilized with 0.2% Triton X-100 (50 µL) for 10 min at room temperature and incubated for 3 min with 10 µL of DAPI by placing a coverslip over the cells to facilitate uniform diffusion of stain. The stained cells were observed under (Nikon Eclipse, Inc, Japan) fluorescent microscope.

Cell Cycle Distribution by Flowcytometry

HepG2 cells (2×10^5) were cultured in 6-well plates overnight and then treated with IC_{50} concentrations of ZnONPs for 24, 48, and 72 h. Doxorubicin (0.40 mg/mL) was used as a positive control. Cells were harvested by centrifugation, washed with ice-cold PBS, and then resuspended with ice-cold 70% ethanol overnight. The cells were treated with 10 µg/mL of RNase at 37 °C, then spun down and stained with propidium iodide (40 µg/mL) for 30 min. The DNA content was analyzed by flow Cytometry (BD Facs), according to the manufacturer instruction.

Statistical Analysis

Data were expressed as mean ± standard deviation (SD, n = 3). Statistical differences compared between treated groups and the untreated group were analyzed by one-way analysis of variance (ANOVA) and followed by Turkey HSD with IBM SPSS version 17.0 (SPSS Inc., USA).

Results and Discussion

Characteristics of the Synthesised ZnONPs

In recent years, the development of eco-friendly ZnONPs has gained special attention due to the wide range of biomedical and physiochemical applications. Since ancient times, ZnO has been broadly studied and used to treat many bacterial infections; it improves wound healing without scarring and applied in medicinal device coatings. In the present study, ZnONPs have been synthesised from fungal extracts of *A. niger* which acts as reducing as well as stabilizing and capping agent. On addition of fungal extract to zinc ion, the color of the cell filtrates showed a gradual change in color towards pale yellow to dark brown which indicates the formation of NPs. Controls (without zinc ion) exhibited no change in color of the cell filtrate in the same experimental condition of incubation and there was no precipitation or aggregation was observed even after the incubation of ZnONPs for 2–3 weeks.

The UV–Vis Spectrophotometer technique was used to measure the structural characterization of nanoparticles by determines the absorbance. In the present study, ZnONPs were synthesised using the fungal biomass of *A. niger* and its UV–visible spectrum was shown in Fig. 1. It represents the characteristic peak of ZnONPs with absorption maxima of 390 nm. Consequently, these ZnONPs absorption spectra will have a solid blue shift signifying these particles should not noteworthy in size than the exciton Bohr radius. Hassan et al. [18] informed that the extracellular biosynthesis of zinc acetate using *A. niger* involves the bioreduction of zinc ions in the culture filtrate. Similar to this, the study of Jamdagni et al. [19] observed the UV spectrum range of ZnONPs is 320–390 nm.

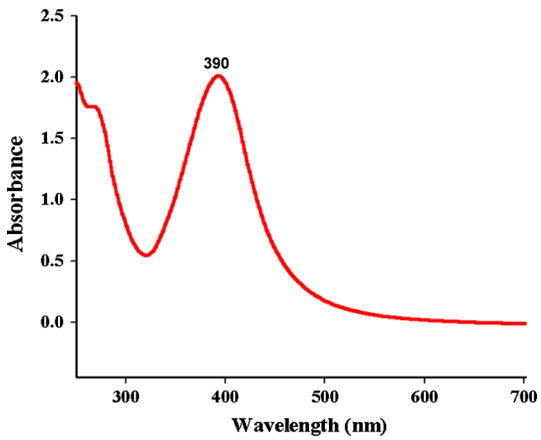

Fig. 1 UV–Vis spectra of synthesised ZnONPs from *A. niger*. The strong absorption spectrum of ZnONPs exhibited at 390 nm

The green synthesised ZnONPs were analyzed through FTIR to find out the interfaces between zinc oxide and bioactive compounds of fungus extract. It was performed to identify the organic functional groups or possible biomolecules involved in the ZnONPs synthesis (Fig. 2). In FT-IR spectrum, the peak observed at 2853.17 cm^{-1} corresponding to C–H stretching vibrations and the peak observed at 1741 cm^{-1} and 1105.98 cm^{-1} responding to C=O stretching vibration of the aldehyde group, whereas the C=C stretching vibrations of IR spectrum observed at 1629.55 cm^{-1}. The peak at 1442.99 cm^{-1} corresponded to O–H bending whereas the C=H bending vibrations of the IR spectrum observed at 1383.68 cm^{-1} and O=H bending vibrations of IR spectrum observed at 945.915 cm^{-1}. The peak observed at 1629.55 cm^{-1} is due to –C=C– aromatic stretching of fungal biomass. These findings suggest that fungal mediated NPs were synthesised by two different processes such us reduction and capping. At first, metal ions are reduced into respective metal NPs, and secondly, capping of the synthesised NPs occurs. Along these lines, the strong aromatic ring and carboxylic acid appearance in FTIR band are responsible for ZnONPs.

DLS is an emerging and vastly used technique for calculating the hydrodynamic diameter of nanoparticle suspensions based on Brownian movements exhibited by the particles. The average hydrodynamic diameter as calculated by DLS is 74 nm and the polydispersity index (PDI)

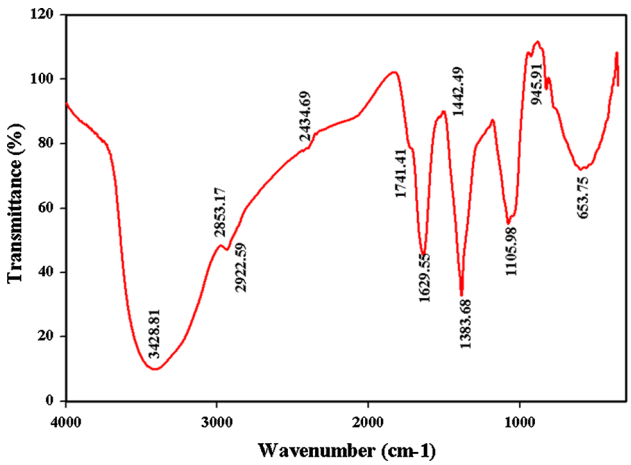

Fig. 2 FTIR spectrum of ZnONPs synthesised from *A. niger*. The strong aromatic ring and carboxylic acid appearance in FTIR band is responsible for the synthesis of ZnONPs from fungal biomass

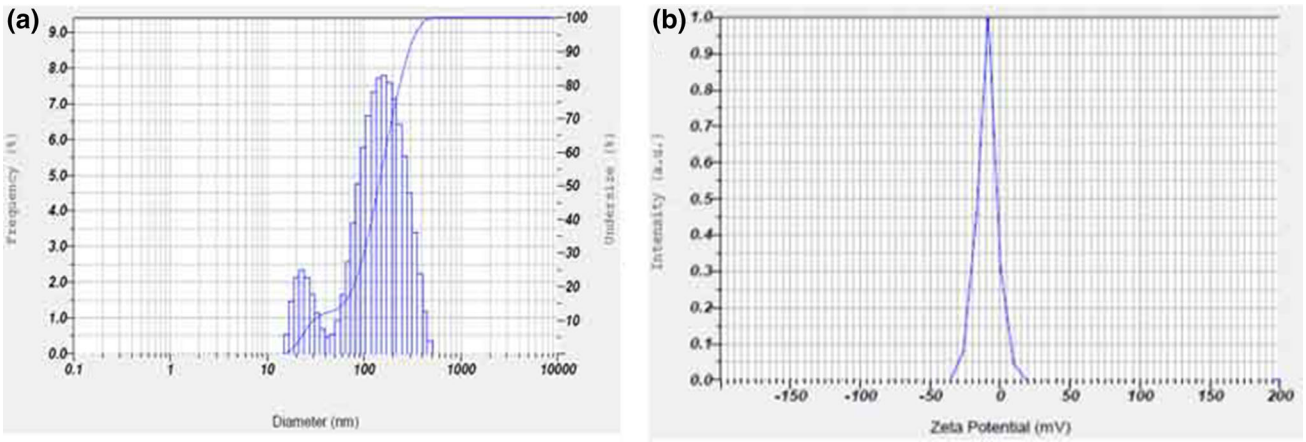

Fig. 3 DLS analysis **a** particle size distribution, **b** zeta potential of ZnONPs synthesized from *A. niger*. The fungal mediated ZnONPs were polydispersed in nature with the average size of 74 nm and the potential value was found to be −11 mV

was found to be 0.543 (Fig. 3a). The presence of the zeta potential values for the ZnONPs is − 11 mV indicating the stability of the NPs (Fig. 3b). Dhoble and Kulkarni [20] have documented a similar pattern for stretching vibration of fungal biomass of *A. niger*. The green synthesised ZnONPs material was characterized by XRD and reflex pattern are shown in Fig. 4. The peaks at 2θ for 21.68°, 26.31°, 31.06°, 37.37°, 43.76°, 55.22°, and 64.68° were assigned to (100), (002), (101), (102), (110), (103), and (200) of ZnONPs, indicating that the samples were polycrystalline nature (JCPDS 5-0664). XRD spectra indicate that the synthesised ZnONPs crystal has complex structural features. The same line of XRD pattern was documented by Hernndez-Melendez et al. [21]. Figure 5 shows the surface morphology and topological feature of the nanomaterials were examined by scanning electron microscope (SEM), transmission electron microscopy (TEM) and selected area diffraction pattern (SAED). SEM analysis confirmed that the synthesised particles were compactly arranged and

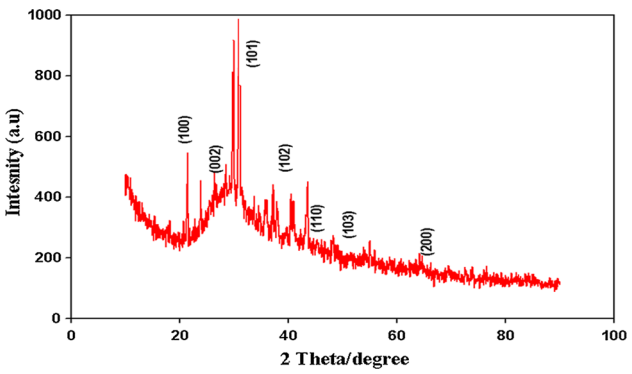

Fig. 4 XRD pattern of ZnONPs synthesised from *A. niger*. The intense peak of the XRD pattern was indicating the polycrystalline nature of green synthesised particles

almost rod and cluster in shape. Similarly, the TEM image of green synthesised ZnONPs by *A. niger* revealed that 80–110 nm. It was showed that the particles are well aggregated with rod and cluster in shape. The morphological features of ZnONPs appear a close resembles *A. niger* mediated zinc oxide nanoparticles [22].

Radical Scavenging Potential of Green Synthesised ZnONPs

In the present investigation, the anti-radical and anti-oxidant activity of biologically synthesised ZnONPs was revealed by employing DPPH and ATBS asssy. The percentage of inhibition of the antioxidant activity of ZnONPs was compared with the standard ascorbic acid and the results are shown in Fig. 6a, b. Maximum inhibition of 57.74% was obtained at 100 µg/mL concentration of ZnONPs to reveal that a higher antioxidant activity, whereas, 13.95% inhibition was achieved for a lower concentration of 5 µg/mL. On the other hand, ABTS assay proved that the ZnONPs has a higher potential to scavenging activity, and its scavenging activity presented in Fig. 6b. Maximum inhibition of 73.58% was obtained at 100 µg/mL concentration of ZnONPs revealing a higher antioxidant activity of green synthesised NPs. 11.23% inhibition was achieved for a lower concentration of 5 µg/mL.

ZnONPs has expressed an effective free radical quenching ability which shows that the percentage of inhibition increases with increasing concentration in a concentration-dependent manner. Thus the ZnONPs has shown good potential in quenching the deleterious free radicals and it was found to have a higher inhibition capacity against DPPH than ATBS. This study has confirmed that the notable antioxidant potential of biologically

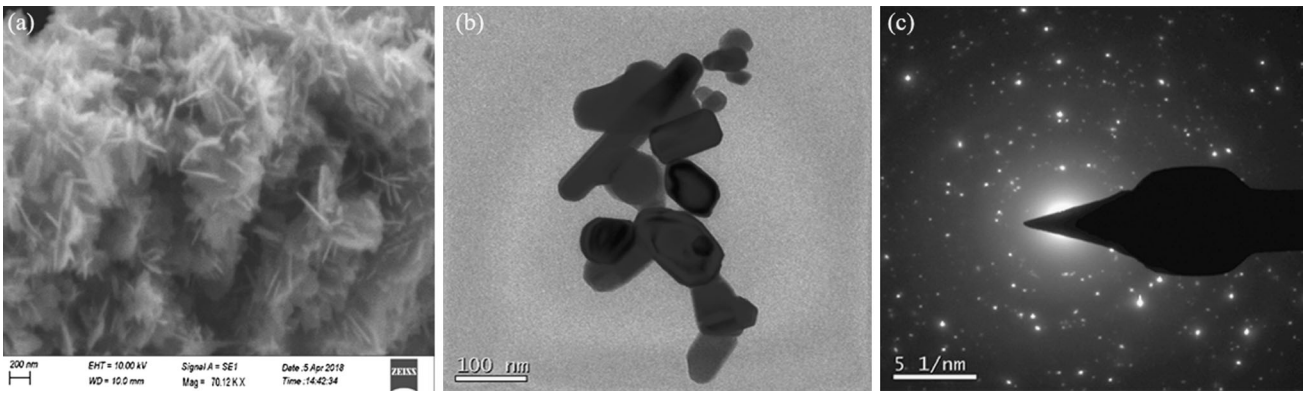

Fig. 5 SEM, TEM and SAED image of ZnONPs synthesised from *A. niger*. The synthesized ZnONPs was showing the rod and cluster shape, and the size ranged from 80–110 nm (**a**, **b**). SAED spots revealed the various crystallographic planes of FCC structure of Zinc (**c**)

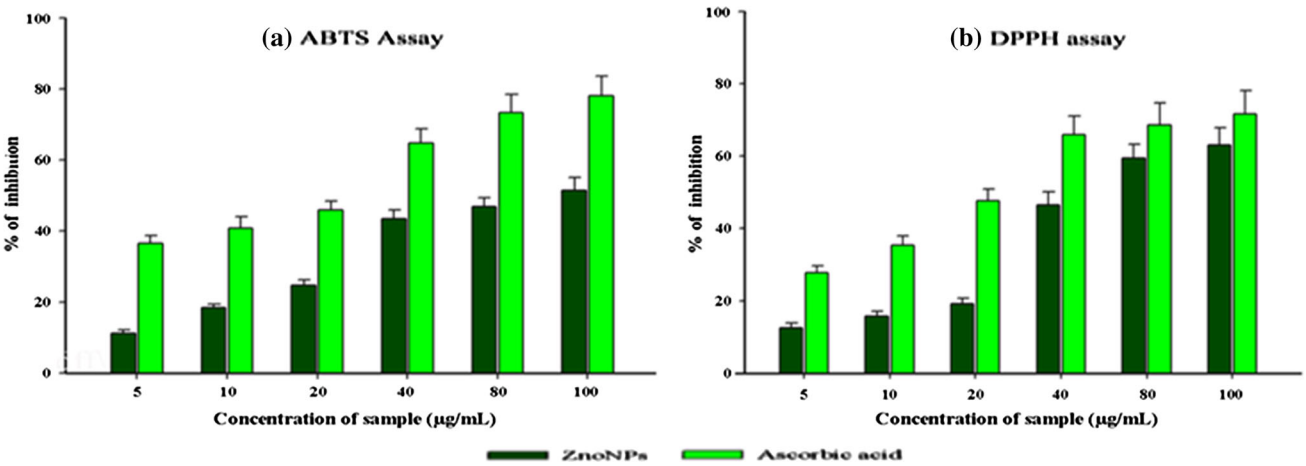

Fig. 6 Percentage inhibition of **a** ABTS+. **b** DPPH radical by various concentrations of ZnONPs compared with standard Ascorbic Acid. The free radical scavenging activity was increased in a dose dependent manner

synthesised ZnONPs and the free radical quenching ability of ZnONPs might be due to the functional groups and biologically active constituents of the fungal biomass. It was understood that the bioactive components involve in the donation of hydrogen atoms to inhibit the free radical reaction [23]. The result indicates the antioxidant activity of ZnONPs has been promoted by the bio-components present in the fungal biomass of *A. niger* as the FTIR results also confirmed the possibility of the presence of a wide range of functional groups.

Antimicrobial Activity of Myco-Synthesised ZnONPs

The notable antimicrobial activity of myco synthesised ZnONPs has been well-demonstrated against a broad spectrum of bacterial strain and clinical isolated multidrug-resistant pathogens. In the present study, human pathogenic gram-negative bacterial strains such as *E. coli, P. aeruginosa, K. pneumoniae, and E. aerogenes* were tested against the synthesised ZnONPs from *A. niger*. It shows the superior antimicrobial activity against tested human pathogens and the results were presented in Fig. 7. ZnONPs significantly inhibited the growth of *P. aeruginosa* (28.81 mm), *K. pneumoniae* (23.69 mm), *E. coli* (21.90 mm) and *E. aerogenes* (19.53 mm) at a test concentration of 500 µg/mL. This antibacterial potential varied among the gram-negative pathogenic microbes tested. This might be due to variation in the structural architecture of bacterial cell wall and particle size surface area to volume ratio of ZnONPs. The most astounding antimicrobial activity was recorded against *P. aeruginosa* and outcome was in good agreement with the prior investigation [24, 25]. The results are in agreement with the recent study, which showed that metal NPs are lead to changes in

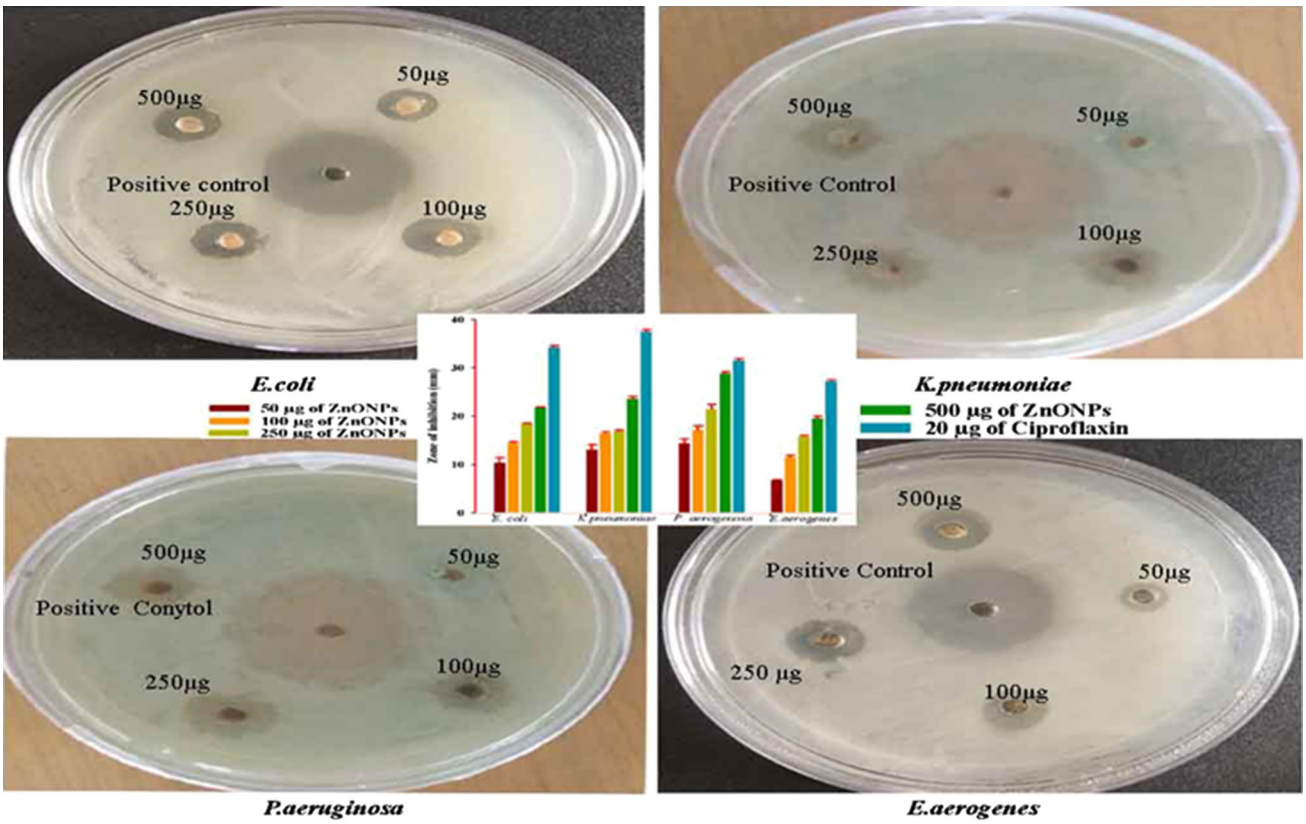

Fig. 7 Antimicrobial activity of ZnONPs against human pathogenic bacteria strain by well diffusion assay. Different concentration of ZnONPs (50–500 µg) significantly inhibited the growth of *P. aeruginosa*, *K. pneumoniae*, *E. coli* and *E. aerogenes*

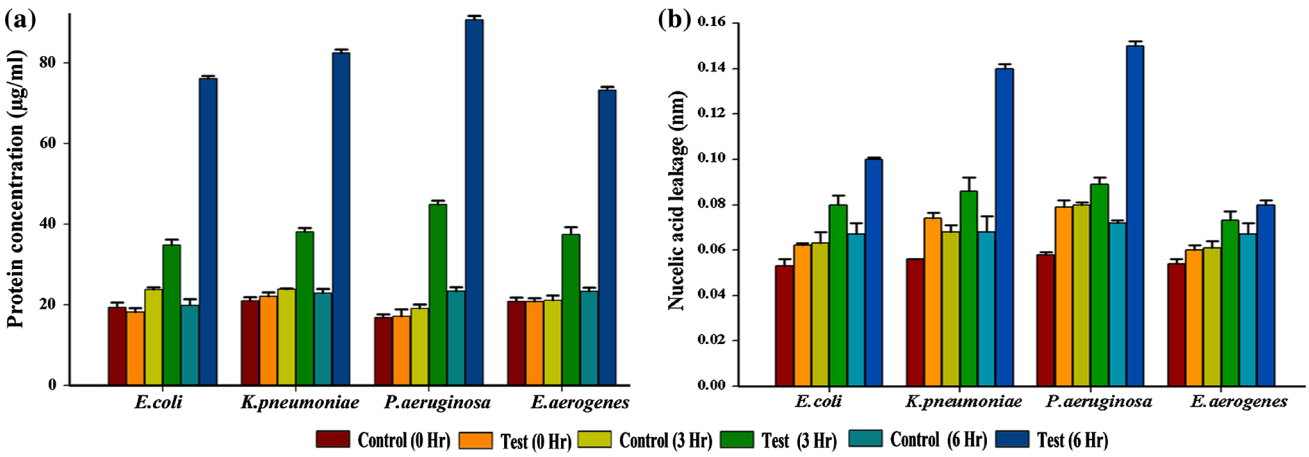

Fig. 8 Cytoplasmic leakage **a** protein, **b** nucleic acid content from ZnONPs treated human pathogenic bacterial strain. ZnONPs treated bacterial cells showed the high amount of intracellular cytoplasmic content than the control cell as can be seen from increased OD value

biological activities including ROS thereby causes membrane damage leading to cell death [26].

Screening of Membrane Leakage of Proteins and Nucleic Acid

Protein leakage from the ZnONPs treated bacterial cells were almost the same as that from cells in the control group

at the beginning of the experiment (Fig. 8). At 3 h after treatment, the ZnONPs treated bacterial cells leaked nearly 33–46 g/mL protein whereas the untreated cells have a similar level of leakage. At 6 h after incubation, the ZnONPs treated bacterial sample showed a higher level of protein leakage than the untreated bacterial strain. Interestingly, *P. aerogenosa* cells showed highest amount of protein leakage (93.74 µg/mL) followed by *K. pneumoniae* (89.12 µg/mL), *E. coli* (72.19 µg/mL) and *E. aerogenes* (63.25 µg/mL) at 6 h after treatment with ZnONPs. On the other hand, the nucleic acid leakage from NPs treated cells and the control cells were almost the same. The bacterial cells exposed to ZnONPs treatment gave rise to the increased release of nucleic acids, which was more marked with *P. aerogenosa* followed by, *K. pneumoniae*, *E. coli* and *E. aerogenes* at 3 and 6 h after treatment with ZnONPs. However, the control of bacterial cells showed lower levels of nucleic acid leakage than the ZnONPs treated bacterial strains.

Several pieces of scientific literature show that the leakage of cytoplasmic contents is a characteristic feature for cytoplasmic membrane damage [15, 27]. Due to the interaction of ZnONPs with the bacterial cell membrane, it loses cell membrane integrity leading to the discharge of intracellular contents such as reducing sugar, protein and nucleic acid content. The findings of this study clearly show that enhanced leakage of intercellular protein was found to be higher in ZnONPs treated cells compared to untreated cells. ZnONPs treated *P. aeruginosa* showed significantly higher protein leakage compared to *E. aerogenes*. Similarly, ZnONPs treated *P. aeruginosa* showed significantly higher nucleic acid leakage compared to *E. aerogenes*. This difference in the leakage of the cytoplasmic profile might be attributed to the thickness of the peptidoglycan layer of the bacterial cell wall. An essential role of the peptidoglycan layer is to protect against antibacterial agents such as antibiotics, toxins, chemicals, and enzymes [28]. In the same way, Steffy et al. [29] found that protein leakage was significantly higher in gram-negative bacteria. Wang et al. [30] documented that the

Table 1 The IC_{50} values of ZnONPs treated non-cancerous and cancer cell lines. Cytotoxic effect of ZnONPs was investigated in HEK-293 and HepG2 cell lines for 24 h to 72 h of treatment were evaluated by MTT assay. Each point is the mean value of three replicates

Treatment	IC_{50} (µg/mL)
HEK-293 cells	> 100
HepG2 + ZnONPs (24 h)	26.75 ± 1.04
HepG2 + ZnONPs (48 h)	22.29 ± 0.35
HepG2 + ZnONPs (72 h)	19.16 ± 0.32
HepG2 + doxorubicin (72 h)	5.35 ± 1.01

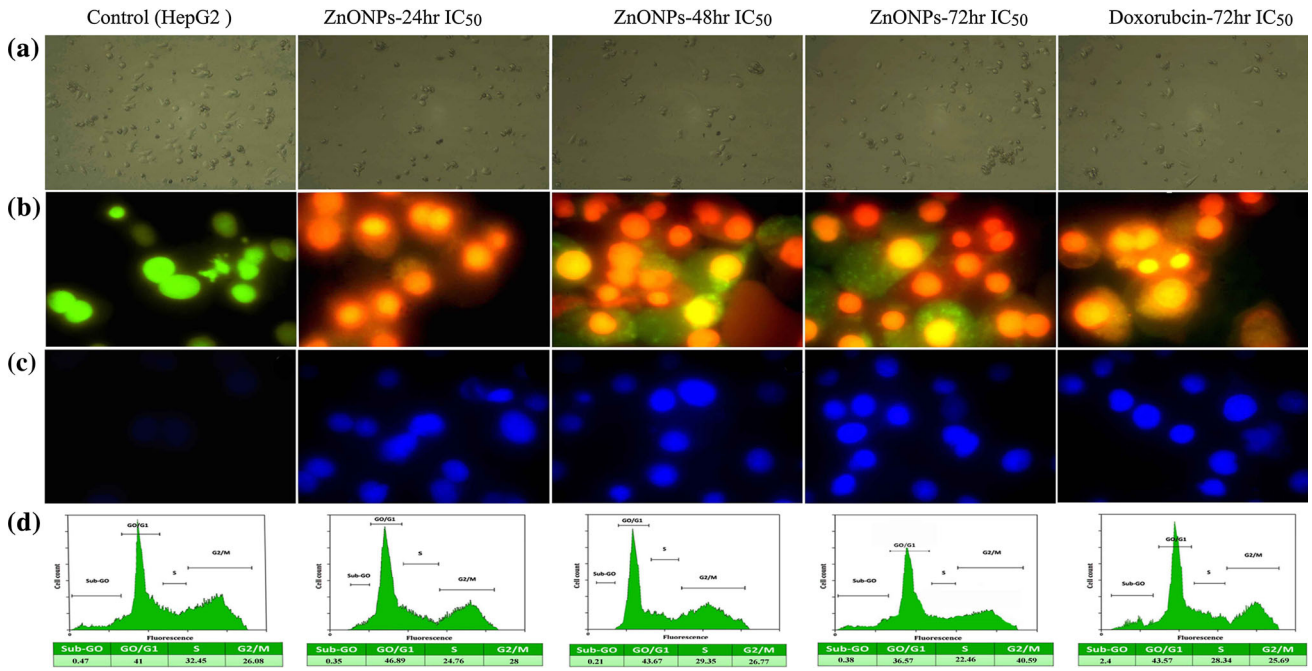

Fig. 9 Cell growth, apoptosis and cell cycle analysis in ZnONPs treated HepG2 cells. **a** Using the MTT assay, ZnONPs treated HepG2 cells displayed a reduced growth compared to control and standard drug doxorubicin. **b** Apoptotic morphology detection by acridine orange/ethidium bromide (AO/EB). **c** DAPI fluorescent staining of HepG2 cells treated. **d** FACS analysis revealed that ZnONPs treated HepG2 cells showed an increased number of cells in G_0/G_1 phase compared to control and standard drug

cytoplasmic leakage from the bacteria cells increased along with the increasing concentration of ZnONPs. It showed the coherence with the antibacterial effect of ZnONPs against various gram-negative bacteria. Altogether, our results were consistent with those of previous studies [31, 32] showing that the mycosynthesised ZnONPs could distort and disrupt the bacterial membranes, consequently leading to intracellular leakage of cytoplasmic content of protein and nucleic acid.

Cytotoxic Potential of Green Synthesised ZnONPs

Green synthesised ZnONPs has unique physiochemical properties such as biocompatibility, tremendous selectivity, remarkable cytotoxicity, and accessible synthesis could be a promising antibacterial and anticancer candidate. However, the anticancer activity of ZnONPs from filamentous fungi *A. niger* has not been well established. The anticancer effect of the green synthesised ZnONPs from *A. niger* was evaluated in both cancer and normal cell line by MTT assay and the results were shown in Table 1 and Fig. 9a. The results show that ZnONPs have a defendable anticancer activity with half-maximum concentration (IC_{50}) values of 26.75 ± 1.04 µg/mL (24 h), 22.29 ± 0.35 µg/mL (48 h) and 19.16 ± 0.32 µg/mL (72 h) and the IC_{50} value of doxorubicin was found to 5.35 ± 1.01 (72 h). On the other hand, ZnONPs was not cytotoxic at the tested concentrations (50 µg/mL) towards the HEK-293 cells. Based on the IC_{50} value, 72 h incubation of ZnONPs was found to be the dominant cytotoxic activity against HepG2 cells and it showed a higher percentage of growth inhibition at lower concentrations. These results are in line with Baskar et al. [33] documented the anti-cancer activity of ZnO conjugated nanobiocomposite against MCF-7 cell line. Taken together, our findings revealed that ZnONPs from the fungal biomass of *A. niger* effectively inhibited the cell viability in a dose and time-dependent manner.

Further, ZnONPs treated cells displayed remarkable apoptotic features in nucleus and cytoplasm. The apoptotic changes of ZnONPs treated HepG2 were stained by AO/Etbr and the results were shown in Fig. 9b. The untreated control cells were appeared as mostly green with a well intact nucleus, whereas the cells treated with IC_{50} concentration of ZnONPs displayed orange and red colored nuclei, which confirmed the induction of apoptosis in HepG2 cells by ZnONPs. This result has further strengthened the apoptotic enhancing effects of ZnONPs was accomplished by DAPI staining (Fig. 9c). It was found that the numbers of apoptotic cells were higher in ZnONPs treated cells than control cells. A well-defined apoptotic body formation and nuclear fragmentation were observed in the cells treated for 72 h incubation, whereas, IC_{50} of 24 and 48 h incubated cells exhibited a moderate apoptotic feature in HepG2. Figure 9d illustrates the cell cycle progression of HepG2 cells were incubated with IC_{50} concentration of ZnONPs using flow cytometry. It was found that ZnONPs efficiently arrested the cell cycle at the G_0/G_1 phase. This observation is in agreement with recent studies on Majeed et al. [34] which showed that fungal-derived ZnONPs induced the apoptosis in a dose-dependent manner. ZnONPs can selectively target and kill cancerous cells, making them a favorable anticancer candidate. Extensive study has revealed that fungi formulated ZnONPs were regulated the oxidative stress, DNA replication process, DNA repair mechanism, cell cycle progression and induces apoptosis in many types of a cancer cell line [35, 36]. In addition, various secondary metabolites from *A. niger* have been used in medicine for their tumor-suppressing, anticancer, and immunosuppressant activities. According to above-cited information; the results of the study concluded that the ZnONPs prepared from *A. niger* had the bioactive compounds with antibacterial, antioxidant and anticancer potential. This study is an innovator work and further study should be carried out for the development of the new drug formulation.

Conclusion

In the present study, we described the synthesised ZnONPs from fungal biomass of *A. niger* using zinc acetate as a reducing agent. Moreover, during characterization UV–visible spectral peak at 390 nm confirmed the purity of ZnONPs and FTIR results documented the reduction. The synthesised nanoparticles was rod and cluster in shape and crystalline in nature with a range 80–130 nm as evident by DLS, XRD, SEM, and TEM. In vivo anticancer study shows that ZnONPs are able to induce time-dependent cytotoxic activity, ROS generation, and apoptosis. Taken together, we conclude that ZnONPs from *A. niger* could be an effective therapeutic agent for the treatment of cancer.

References

1. J. Jeevanandam, A. Barhoum, Y. S. Chan, A. Dufresne, and M. K. Danquah (2018). *Beilstein J. Nanotechnol.* **9**, 1050–1074. https://doi.org/10.3762/bjnano.9.98.
2. O. Bondarenko, A. Ivask, A. Kakinen, I. Kurvet, and A. Kahru (2013). *PLoS ONE* **8**, e64060. https://doi.org/10.1371/journal.pone.0064060.
3. A. Nejabatdoust, A. Salehzadeh, H. Zamani, and Z. M. Shoeili (2019). *J. Clust. Sci.* **30**, 329–336. https://doi.org/10.1007/s10876-018-01487-3.
4. P. K. Mishra, H. Mishra, A. Ekielski, S. Talegaonkar, and B. Vaidya (2017). *Drug Discov. Today* **22**, 1825–1834. https://doi.org/10.1016/j.drudis.2017.08.006.

5. B. Malaikozhundan, B. Vaseeharan, S. Vijayakumar, K. Pandiselvi, M. A. Kalanjiam, K. Murugan, and G. Benelli (2017). *Microb. Pathog.* **104**, 268–277. https://doi.org/10.1016/j.micpath.2017.01.029.
6. C. Paulussen, J. E. Hallsworth, S. Alvarez-Perez, W. C. Nierman, P. G. Hamill, and D. Blain (2017). *Microb. Biotechnol.* **10**, 296–322. https://doi.org/10.1111/1751-7915.12367.
7. O. S. Zmeili and A. O. Soubani (2007). *QJM Int. J. Med.* **100**, 317–334. https://doi.org/10.1093/qjmed/hcm035.
8. E. Schuster, N. Dunn-Coleman, J. Frisvad, and P. Van Dijck (2002). *Appl. Microbiol. Biotechnol.* **59**, 426–435. https://doi.org/10.1007/s00253-002-1032-6.
9. H. L. Holland (1997). *Adv. Appl. Microbiol.* **44**, 125–165.
10. A. K. Gade, P. Bonde, A. P. Ingle, P. D. Marcato, N. Duran, and M. K. Rai (2008). *J. Biobased Mater.* **2**, 243–247. https://doi.org/10.1166/jbmb.2008.401.
11. K. Kathiresan, N. M. Alikunhi, S. Pathmanaban, A. Nabikhan, and S. Kandasamy (2010). *Can. J. Microbiol.* **56**, 1050–1059. https://doi.org/10.1139/W10-094.
12. R. Re, N. Pellegrini, A. Proteggente, M. Yang, and C. Rice-Evans (1999). *Free Radic. Biol. Med.* **26**, 1231–1237.
13. K. Shimada, K. Fujikawa, K. Yahara, and T. Nakamura (1992). *J. Agric. Food Chem.* **40**, 945–948.
14. J. F. Hernandez-Sierra, F. Ruiz, D. C. Pena, F. Martinez-Gutierrez, A. E. Martinez, and A. D. Guillen (2008). *Nanomed. Nanotechnol.* **4**, 237–240. https://doi.org/10.1016/j.nano.2008.04.005.
15. S. H. Kim, H. S. Lee, D. S. Ryu, S. J. Choi, and D. S. Lee (2011). *Korean J. Microbiol. Biotechnol.* **39**, 77–85. https://doi.org/10.5897/AJMR2016.7908.
16. A. Alvarez-Ordonez, O. Alvseike, M. K. Omer, E. Heir, L. Axelsson, A. Holck, and M. Prieto (2013). *Int. J. Food Microbiol.* **161**, 220–230. https://doi.org/10.1016/j.ijfoodmicro.2012.12.008.
17. M. B. Hansen, S. E. Nielsen, and K. Berg (1989). *J. Immunol. Methods* **119**, 203–210. https://doi.org/10.1016/0022-1759(89)90397-9.
18. S. S. M. Hassan, W. I. M. El-Azab, H. R. Ali, and M. S. M. Mansour (2015). *Adv. Nat. Sci. Nanosci. Nanotechnol.* **6**, 045012. https://doi.org/10.1088/2043-6262/6/4/045012.
19. P. Jamdagni, P. Khatri, and J. S. Rana (2018). *King Saud Univ. Sci.* **30**, 168–175. https://doi.org/10.1016/j.jksus.2016.10.002.
20. S. M. Dhoble and N. S. Kulkarni (2016). *Sch. Acad. J. Biosci.* **11**, 1022–1031. https://doi.org/10.21276/sajb.2016.4.11.9.
21. D. Hernndez-Melendez, E. Salas-Tellez, A. Zavala-Franco, G. Tellez, A. Mendez-Albores, and A. Vazquez-Duran (2018). *Materials* **11**, 1265. https://doi.org/10.3390/ma11081265.
22. V. N. Kalpana, B. A. S. Kataru, N. Sravani, T. Vigneshwari, A. Panneerselvam, and V. Devi Rajeswari (2018). *OpenNano* **3**, 48–55. https://doi.org/10.1016/j.onano.2018.06.001.
23. E. E. Elemike, D. C. Onwudiwe, O. E. Fayemi, A. C. Ekennia, E. E. Ebenso, and L. R. Tiedt (2017). *J. Clust. Sci.* **28**, 309–330. https://doi.org/10.1007/s10876-016-1087-7.
24. L. L. Duffy, M. J. Osmond-McLeod, J. Judy, and T. King (2018). *Food Control* **92**, 293–300. https://doi.org/10.1016/j.foodcont.2018.05.008.
25. P. Kalyani, B. K. Lakshmi, G. Dinesh Reddy, and K. P. Hemalatha (2018). *Int. J. Curr. Res.* **7**, 788–791.
26. A. Manke, L. Wang, and Y. Rojanasakul (2013). *Biomed. Res. Int.*. https://doi.org/10.1155/2013/942916.
27. T. O. Ajiboye, A. O. Mohammed, S. A. Bello, I. I. Yusuf, O. B. Ibitoye, H. F. Muritala, and I. B. Onajobi (2016). *Microb. Pathog.* **95**, 208–215. https://doi.org/10.1016/j.micpath.2016.03.011.
28. R. Sinha, R. Karan, A. Sinha, and S. K. Khare (2011). *Bioresour. Technol.* **102**, 1516–1520. https://doi.org/10.1016/j.biortech.2010.07.117.
29. K. Steffy, G. Shanthi, A. S. Maroky, and S. Selvakumar (2018). *J. Infect. Public Health* **11**, 463–471. https://doi.org/10.1016/j.jiph.2017.10.006.
30. Y. W. Wang, A. Cao, Y. Jiang, X. Zhang, J. H. Liu, Y. Liu, and H. Wang (2014). *ACS Appl. Mater. Interfaces* **6**, 2791–2798. https://doi.org/10.1021/am4053317.
31. A. Aditya, S. Chattopadhyay, D. Jha, H. K. Gautam, S. Maiti, and M. Ganguli (2018). *ACS Appl. Mater. Interfaces* **10**, 15401–15411. https://doi.org/10.1021/acsami.8b01463.
32. T. C. Dakal, A. Kumar, R. S. Majumdar, and V. Yadav (2016). *Front. Microbiol.* **7**, 1831. https://doi.org/10.3389/fmicb.2016.01831.
33. G. Baskar, J. Chandhuru, K. S. Fahad, A. S. Praveen, M. Chamundeeswari, and T. Muthukumar (2015). *J. Mater. Sci. Mater. Med.* **26**, 43. https://doi.org/10.1007/s10856-015-5380-z.
34. S. Majeed, M. Danish, and F. S. Norazmi (2018). *Adv. Sci. Eng. Med.* **1**, 551–556. https://doi.org/10.14302/issn.2377-2549.jndc-18-2116.
35. K. S. Siddiqi, A. Ur Rahman, and A. Husen (2018). *Nanoscale Res Lett.* **13**, 141. https://doi.org/10.1186/s11671-018-2532-3.
36. M. Arakha, J. Roy, P. S. Nayak, B. Mallick, and S. Jha (2017). *Free Radic. Biol. Med.* **110**, 42–53. https://doi.org/10.1016/j.freeradbiomed.